ANTIOXIDANTS & REDOX SIGNALING
Volume 12, Number 1, 2010

DOI: 10.1089/ars.2008.2418

Mitochondrial Complex III Defects Contribute to Inefficient Respiration and ATP Synthesis in the Myocardium of *Trypanosoma cruzi*–Infected Mice

Jian-Jun Wen[1] and Nisha Jain Garg[1,2,3]

Abstract

In this study, we conducted a thorough analysis of mitochondrial bioenergetic function as well as the biochemical and molecular factors that are deregulated and contribute to compromised adenosine triphosphate (ATP) production in the myocardium during *Trypanosoma cruzi* infection. We show that ADP-stimulated state 3 respiration and ATP synthesis supported by pyruvate/malate (provides electrons to complex I) and succinate (provides electrons to complex II) substrates were significantly decreased in left ventricular tissue and isolated cardiac mitochondria of infected mice. The decreased mitochondrial ATP synthesis in infected murine hearts was not a result of uncoupling between the electron-transport chain and oxidative phosphorylation and decreased availability of the intermediary metabolites (*e.g.*, NADH). The observed decline in the activities of complex-I, -IV, and -V was not physiologically relevant and did not contribute to compromised respiration and ATP synthesis in infected myocardium. Instead, complex III activity was decreased above the threshold level and contributed to respiratory-chain inefficiency and the resulting decline in mitochondrial ATP synthesis in infected myocardium. The loss in complex III activity occurred as a consequence of cytochrome *b* depletion. Treatment of infected mice with phenyl-α-*tert*-butyl nitrone (PBN, antioxidant) was beneficial in preserving the mtDNA-encoded cytochrome *b* expression, and subsequently resulted in improved complex III activity, mitochondrial respiration, and ATP production in infected myocardium. Overall, we provide novel data on the mechanism(s) involved in cardiac bioenergetic inefficiency during *T. cruzi* infection. *Antioxid. Redox Signal.* 12, 27–37.

Introduction

Chagas disease is a major human health problem in Latin America (47). It is estimated that 13 million people are infected and 40 million are exposed to the risk of *Trypanosoma cruzi* infection in countries in which it is endemic. In ~30% of the infected individuals, symptomatic chronic chagasic cardiomyopathy developed with a progressive global ventricular dilation, arrhythmia, and contractile dysfunction (24).

The myocardial contractile function is essentially supported by oxidative phosphorylation (33), in which respiratory electron flow in the inner membrane of the mitochondria is coupled to the F_oF_1 ATP synthase and produces high-energy metabolite ATP (35). Studies with experimental animals infected with *T. cruzi* and biopsies from human patients have shown that mitochondrial alterations, cellular damage, and oxidized proteins and lipids are dominantly present in chagasic hearts with progressive disease (4, 13, 22, 23, 44). The enzymatic activity of the respiratory complexes was compromised in the myocardium (41) and not in other tissues of infected animals (45). Accordingly, a decline in cardiac energy status was noted in experimental models of *T. cruzi* infection (38, 41) and in chagasic humans (16), and it was proposed that mitochondrial dysfunction and energy depletion contribute, at least partially, to myocardial contractile dysfunction during Chagas disease. No detailed studies have; however, been conducted to determine whether and how mitochondrial abnormalities affect the rate of ATP synthesis in chagasic myocardium.

In this study, we aimed to determine whether the bioenergetics of cardiac mitochondria is altered in *T. cruzi*–infected mice, and if such is the case, to identify the subcellular mechanisms that contribute to the dissipation of energy output in

Departments of [1]Microbiology & Immunology and [2]Pathology, and [3]Member of The Institute for Human Infections and Immunity, The Center for Biodefense & Emerging Infectious Diseases, and The Sealy Center for Vaccine Development, University of Texas Medical Branch, Galveston, Texas.

infected myocardium. We treated infected mice with phenyl-α-*tert*-butyl nitrone (PBN, antioxidant) to determine whether oxidative stress affects the mitochondrial respiration and coupled oxidative phosphorylation capacity in chagasic myocardium. PBN reacts with short-lived oxygen and carbon-centered radicals at the nitrone double bond and result in the formation of relatively stable nitroxide that does not propagate the destructive radical chain reaction (11). We chose PBN because inflammatory responses elicited by *T. cruzi* infection (6) and ROS production by mitochondria (46) can cause oxidative stress, and PBN treatment was found to be beneficial in preventing the myocardial oxidative damage in infected mice (42). The findings in the current study demonstrate that a decline in mitochondrial DNA-encoded cytochrome *b* (cyt b) expression resulted in compromised complex III activity that led to inefficient electrochemical gradient and decreased ATP synthesis in infected myocardium. Infected mice treated with PBN exhibited improved cardiac mitochondrial respiration and ATP synthesis associated with preservation of mtDNA, cyt b expression, and complex III activity. We discuss the mechanism(s) involved in bioenergetic inefficiency of the heart during *T. cruzi* infection.

Materials and Methods

Mice and parasites

Six-to-eight-week-old male C3H/HeN mice (Harlan Labs, Indianapolis, IN) were infected with *T. cruzi* trypomastigotes (SylvioX10/4 strain, 10,000/mouse, IP). Mice were treated with PBN beginning day 0 (50 mg/kg body weight, IP., alternate days) until the end of the study. Mice were killed at day 27 to 35 after infection (acute phase). The UTMB Animal Care and Use Committee had approved all animal experiments performed in this study.

Isolation of mitochondria

All solutions were prepared with highly pure chemicals (Sigma-Aldrich, St. Louis, MO) devoid of divalent cations in HPLC grade H_2O. Freshly harvested heart ventricular tissues were washed with ice-cold HMSB medium (10 m*M* HEPES pH 7.4, 225 m*M* mannitol, 75 m*M* sucrose, and 0.2% fatty acid free BSA) and resuspended in HMSB containing 200 U/ml collagenase (1:20 ratio, tissue/buffer). Tissues were homogenized in a dounce homogenizer, incubated for 3 min, and 1 m*M* EGTA added to stop collagenolysis and prevent mitochondrial Ca^{2+} uptake (43). Samples were centrifuged sequentially at 480 *g* and 8,000 *g* and pelleted mitochondria kept on ice without dilution. To evaluate the contamination of other organelles in isolated mitochondria, the enzymatic activities of glucose-6-phosphatase (G-6-Pase, endoplasmic reticulum marker) (14) and acid phosphatase (APase, peroxisome marker) (21) were measured according to published procedures. Protein content was measured with the Bradford method.

In some experiments, mitochondria were subjected to Percoll density-gradient centrifugation (34). In brief, the mitochondrial pellet (above) was suspended in 15% Percoll, layered on top of 23% and 40% Percoll, and centrifuged at 30,700 *g*. The mitochondrial fraction at the lower interface was suspended in HMSB buffer (1:20, vol/vol), and centrifuged at 14,000 *g*. The pellet was washed again, centrifuged at 8,100 *g*, and used for various assays. All centrifugations were performed for 10 min at 4°C.

Oxygen consumption and respiration

Mitochondrial respiration was assessed by using a Mitocell S200A Micro Respirometry System (Strathkelvin Instruments, Motherwell, U.K.). In brief, a microcathode oxygen electrode was calibrated and, after baseline measurements, mitochondria (200 μg), suspended in 0.5 ml MSP medium (225 m*M* mannitol, 75 m*M* sucrose, 20 m*M* K_2HPO_4/KH_2PO_4 buffer, pH 7.4), were added to the mitocell. The substrate-stimulated oxygen consumption (state 4) was measured in the presence of 10 m*M* pyruvate/2.5 m*M* malate (pyr/mal), 5 m*M* succinate/6.25 μ*M* rotenone (suc/rot), or 3 m*M* ascorbate/0.25 m*M* *N,N,N,N*-tetramethyl-*p*-phenylenediamine (asc/TMPD). The state 3 oxygen consumption was measured after addition of 230 μ*M* ADP. Respirometry software (Strathkelvin) was used to calculate the respiratory control ratio (RCR). The ADP/O ratio (amount of ADP phosphorylated/O atom consumed) determines the mitochondrial capacity to produce ATP and was calculated by measuring the decrease in O_2 concentration during the rapid burst of state 3 respiration, by using "total" oxygen as defined by Lemasters (18).

To measure myocardial oxygen consumption, we harvested the heart from anesthetized mice and perfused with Kreb's solution to remove blood. Left ventricle tissue was dissected longitudinally, incubated in Kreb's solution at 37°C, 5% CO_2 for 2 h, and oxygen consumption measured as described earlier. To assess *in vivo* mitochondrial respiration, tissue slices were incubated in air-saturated Kreb's solution containing 5 m*M* succinate/6.25 μ*M* rotenone (20).

Mitochondrial ATP production

Freshly isolated mitochondria (15–20 μg protein/μl) were diluted 15-fold (just before use) in reaction buffer (15 m*M* K_2HPO_4/KH_2PO_4 buffer, pH 7.2, 250 m*M* sucrose, 2 m*M* $MgAc_2$, 0.5 m*M* EDTA and 0.5 g/L human serum albumin). In black-bottomed 96-well plates, 140 μl reaction buffer (2.5 μg/ml luciferase, 20-μg/ml D-luciferin and 20 μl substrate) and 20 μl mitochondria (25–50 μg protein) were added. After incubation for 2–3 min to deplete endogenous ATP, 20 μl ADP solution (6 m*M* ADP and 20 μ*M* P1, P5-di(adenosine)-pentaphosphate) was added, and the change in luminiscence recorded by using a Promega Veritas Microplate Luminometer (standard curve, 10 p*M* to 10 μ*M* ATP) (48). The use of highly pure ADP consisting of less than 0.04 μ*M* ATP (Apollo Scientific) was essential to keep the background below 1% of the sample values.

Enzymatic and biochemical assays

Freshly isolated mitochondria (15 μg protein) were used in all assays. Complex I (NADH: ubiquinone reductase) activity was monitored by oxidation of NADH (200 μ*M*) in the presence of 80 μ*M* 2,3-dimethoxy-5-methyl-6-decyl-1, 4-benzoquinone (DB) as electron acceptor (±6.5 μ*M* rotenone, $\varepsilon_{340\,nm}$: 6.1 m*M*/cm). Complex III (ubiquinol: cytochrome *c* reductase) activity was quantitated by the oxidation of 60 μ*M* of reduced DB, by using 50 μ*M* cytochrome *c* (cyt c) as an electron donor (±1 μ*M* antimycin, ε_{550nm}: 19.1 m*M*/cm). To assess the NADH level, isolated mitochondria were incubated

at 55°C for 10 min in 0.2 *M* NaOH (1/10, wt/vol), neutralized by using 0.1 *M* HCl and centrifuged at 12,000 *g* for 10 min. The concentration of NADH in supernatants was determined by the rate of 3-(4,5-dimethylthiazol-2-yl)-2,5-diphenyltetrazolium bromide reduction by alcohol dehydrogenase (yeast type II, Sigma) in the presence of phenazine ethosulfate at 570 nm (19).

Titration curves

Mitochondria were incubated for 5 min with varying concentrations of complex I (0–100 n*M* rotenone) and complex III (0–100 n*M* antimycin) inhibitors. Mitochondria were then energized with pyr/mal or succinate substrates, and the effect of inhibitors on the rate of ADP-stimulated state 3 respiration (by oxigraphy), ATP production (by luciferase-bioluminescence assay) and complex activities (by spectrophotometry) were monitored as described earlier. Threshold rates for the state 3 respiration and ATP production rate were derived from titration curves. Each point of the threshold curve represents the respiratory rate or ATP production rate as a function of the respiratory complex activity.

Cytochrome b *expression*

Cytochrome *b* DNA level was determined by Southern blotting. In brief, heart tissues (50 mg) were subjected to proteinase K lysis, treated with RNase A to remove contaminating RNA and total DNA isolated by phenol/chloroform extraction/ethanol precipitation. Total DNA (3 μg), after digestion with *Eco*RI, was resolved on agarose gel, transferred to membranes, and hybridized with [α^{32}P]-labeled probes for cyt b or 18S ribosomal RNA (41). Images were acquired by using a Storm 860 phosphorimager (Amersham, Piscataway, NJ). To validate the Southern results, total DNA (50 ng) was used as a template, and real-time PCR was performed by using 12.5 μl of Power SYBR-Green PCR Master Mix (ABI) and 0.5 μl of 20 μM specific primer pairs (*cyt b*: forward, 5′-gttcgcagtcatagccacag-3′; reverse, 5′-ggcggaatattaggcttcgt-3′; *GAPDH*: forward, 5′-tggcaaagtggagattgttg-3′; reverse, 5′-ttcagctctgggatgacctt-3′) on a ABI7000 Prism system (Applied Biosystems, Foster City, CA). The threshold cycle (C_t) values were normalized to *GAPDH,* and the relative *cyt b* DNA level was calculated by using the formula $2^{-\Delta Ct}$ where ΔC_t represents the C_t (target)$-C_t$ (control) (12).

To assess *cyt b* mRNA levels with Northern blotting, total RNA from heart tissues (50 mg) was isolated with the guanidinium thiocyanate-phenol-chloroform method (8) and treated with DNase (Ambion, Austin, TX) to remove contaminating DNA. Samples (2.5 μg total RNA) were denatured in 50% formamide/2 *M* formaldehyde, resolved on 1% agarose gel containing 2 *M* formaldehyde in 4-morpholinepropanesulfonic acid (MOPS) buffer. Membranes were hybridized with [α^{32}P]-labeled *cyt b* or *18S ribosomal* cDNA probes and images captured. To validate Northern results by real-time RT-PCR, first-strand cDNA was synthesized from DNase-treated total RNA (2 μg) by using 2.5 units of MuMLV reverse transcriptase (New England Biolabs, Ipswich, MA) and 1 μM poly(dT)$_{18}$ oligonucleotide. The cDNA (2 μl) was used as a template with *cyt b*- or *GAPDH*-specific primers, and a PCR reaction performed on an ABI7000 Prism system (as described earlier). In some instances, RT-PCR was performed by using a thermocycler (Perkin-Elmer, Waltham, MA) and individual amplicons resolved on 1.5% agarose gel.

The cyt b protein level was assessed with Western blotting (13). In brief, isolated mitochondria (15 μg) or the complex III purified from the blue native gel (50 μg loading) (29) were resolved on a 10–15% gradient SDS-polyacrylamide gel, and proteins were transferred to PVDF membrane (BioRad). Membranes were incubated with a rabbit polyclonal antibody against cyt b (1:200 dilution, Santa Cruz), followed by HRP-conjugated anti-rabbit IgG (1:2,000 dilution). Signal was developed by using ECL Western Blotting Detection Reagents (Amersham) and quantitated with densitometry.

Data analysis

Data (mean $\pm$ SD) were derived from at least triplicate observations per sample ($n \geq 9$ animals/group). Results were analyzed for significant differences by using ANOVA and Student's *t* test. The level of significance was accepted at $p < 0.05$.

Results

Our first objective was to isolate intact mitochondria with high purity. We used differential centrifugation and Percoll gradient methods to isolate cardiac mitochondria and evaluated the state 4 and state 3 oxygen consumption as an indicator of mitochondrial integrity. Shown in Fig. 1A is a typical measurement of mitochondrial oxygen consumption by oxigraphy. The rate of pyr/mal (complex I substrates) and succinate (complex II substrate)-stimulated state 4 respiration was significantly higher in Percoll-purified normal cardiac mitochondria as compared with that noted in mitochondria isolated by differential centrifugation (Table 1). No significant difference was observed in ADP-stimulated respiration in substrate-energized cardiac mitochondria, isolated by either of the two methods (Table 1). These results suggest that mitochondria isolated by differential centrifugation were coupled and maintained a high RCR (state 3/state 4 > 4). The measurement of possible contaminants in mitochondria isolated with differential centrifugation indicated that 6% or less of the glucose-6-phosphatase (ER marker) (Fig. 1B) and acid phosphatase (peroxisome marker) activities (Fig. 1C) were present in mitochondrial preparations when compared with that detected in the heart homogenates. We detected no statistically significant difference in citrate synthase activity in different cardiac mitochondrial preparations from normal, infected, and infected/PBN-treated mice (data not shown). Together, these data showed that the differential centrifugation method was efficient for isolation of >94% pure highly coupled mitochondria in different extractions from all experimental groups. All further studies, therefore, were conducted with mitochondria isolated by differential centrifugation, and additional purification by Percoll method was not used.

The myocardial ATP content is compromised in infected mice (42). To determine whether such is the case because of decreased mitochondrial oxidative phosphorylation efficiency, we measured ATP production by using a luciferin/luciferase-based bioluminescence method. The change in luminescence per unit of time (Fig. 2A) was extrapolated to calculate the ATP production (Fig. 2B). The pyr/mal- and succinate-supported ATP production was decreased by 50%

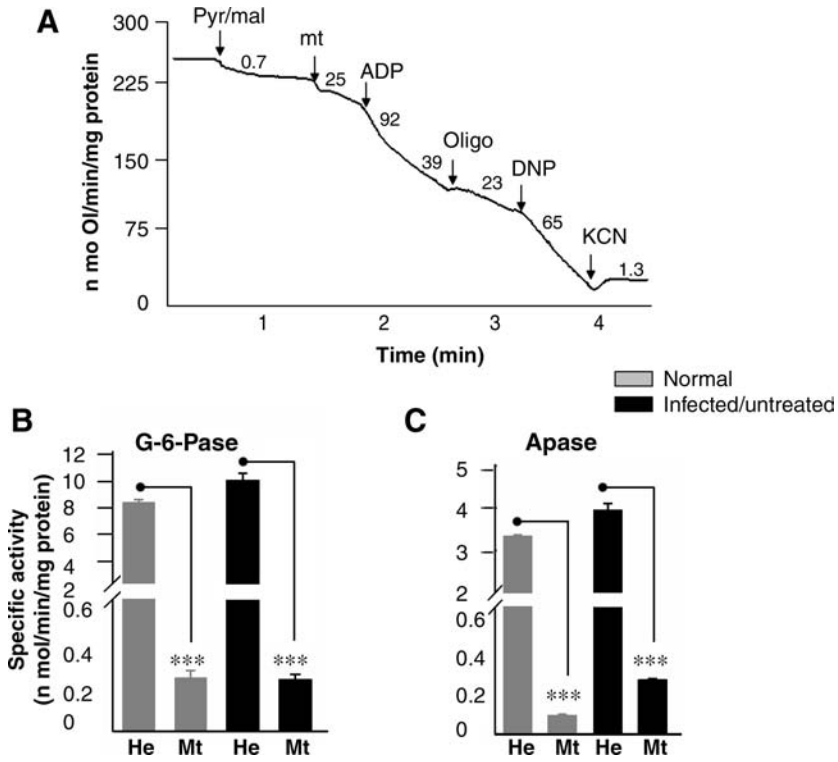

FIG. 1. Isolation of mitochondria of high purity. C3H/HeN mice were infected with *T. cruzi*. Animals were killed during the acute infection phase and cardiac mitochondria were isolated as described in Materials and Methods. (**A**) A typical polarographic measurement with cardiac mitochondria by using a Mitocell S200A Respirometry system. *Arrows*, The time point of addition of substrate (pyr/mal), mitochondria (mt), ADP (stimulates state 3 respiration), oligomycin (oligo, inhibits ATP synthesis and ADP-stimulated state 3 respiration), dinitrophenol (DNP, uncoupler), and KCN (complex IV inhibitor, blocks respiration). The rate of oxygen consumption was calculated as nonomoles of O/min/mg protein. The activities of glucose-6-phosphase (G-6-Pase) (**B**) and acid phosphatase (APase) (**C**) were monitored in isolated mitochondria and heart homogenates ($n = 9$ per group; $^{***}p < 0.001$).

and 44%, respectively, in infected myocardial mitochondria (Fig. 2B, Table 2). The ATP production rate was substantially inhibited by myxothiazol (complex III inhibitor, 87% decline or more) and oligomycin (complex V inhibitor, 75% decline), and completely abolished by complex IV inhibitor (KCN) or mitochondrial uncoupler (DNP). Rotenone (complex I inhibitor) resulted in an 88% or more inhibition of ATP synthesis in pyr/mal-respiring mitochondria, whereas malonate (complex II inhibitor) resulted in a >93% inhibition of the succinate-supported ATP production (Table 2). The inhibition studies confirmed that the observed changes in ATP production in infected myocardium (Fig. 2) are mitochondria specific and dependent on the coupling of respiratory chain and oxidative phosphorylation. The pyr/mal and succinate-supported ATP synthesis in cardiac mitochondria of infected/PBN-treated mice was decreased by only 8–14% as compared with the 44–50% loss detected in infected/untreated mice (Fig. 2). These data suggest that PBN treatment of infected mice was effective in improving the mitochondrial function.

To identify the factors that may contribute to decreased ATP production in infected heart, we first determined the level of intermediate metabolites that provide electron energy for ATP synthesis in isolated cardiac mitochondria. We found no statistically significant difference in the mitochondrial NADH level (Fig. 3A), NAD^+/NADH ratio (Fig. 3B) and succinate metabolism (data not shown) in normal, infected. and infected/PBN-treated mice. suggesting that the availability of an electron donor for ATP synthesis is not compromised in infected myocardium.

Alterations in respiratory complex activities, noted in the chagasic hearts (41, 45), may affect electron-transport efficiency and coupled oxidative phosphorylation. We measured oxygen consumption in isolated mitochondria and heart tissue to evaluate the respiratory efficiency in infected mice. The state 4 respiration supported by pyr/mal, succinate, and ascorbate/TMPD substrates that provide electrons to complex I, II, and IV, respectively (Fig. 4A), and maximal oxygen consumption in presence of dinitrophenol (uncoupler, Fig. 4B)

Table 1. Mitochondria Isolated by Differential Centrifugation Are Coupled

Substrate	*Method*	*Respiration (nmol atom O/min/mg protein)*		*RCR value*
		State 4 (−ADP)	*State 3 (+ADP)*	
Pyruvate + malate	DF	20.11 ± 1.76	93.72 ± 8.01	4.68 ± 0.49
	Percoll	40.58 ± 9.45	92.58 ± 12.84	2.35 ± 0.47
Succinate + rotenone	DF	16.05 ± 3.89	86.08 ± 8.39	5.58 ± 1.22
	Percoll	41.26 ± 4.56	85.58 ± 5.64	2.09 ± 0.24

Cardiac mitochondria from 8-week-old normal mice were isolated by differential centrifugation (DF). Half of mitochondrial fraction was further purified by the discontinuous Percoll gradient method. Mitochondria were incubated with the indicated substrates, and respiration rates were determined with oxigraphy. Respiratory control ratio (RCR) was calculated as the ratios of state 3 rate to state 4 rate. The data (mean ± SD) are representative of three independent experiments ($n = 3$ per experiment/group).

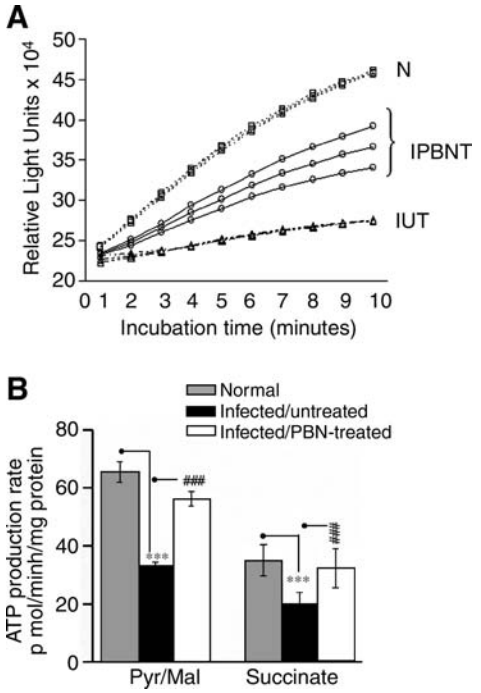

FIG. 2. Isolated cardiac mitochondria were energized with pyruvate/malate (pyr/mal) or succinate substrates, and the rate of ATP production was determined with a luciferin/luciferase-based assay. (**A**) Luminescence curves demonstrating the ATP-production rate in pyruvate/malate–respiring cardiac mitochondria from normal (N), infected/untreated (IUT), and infected/PBN-treated (IPBNT) mice. (**B**) The data from luminescence curves were extrapolated to calculate the ATP production ($n = 9$ per group). The level of significance is shown by $^{***}p < 0.001$ (normal *vs.* infected mice) and $^{\#\#\#}p < 0.001$ (infected/PBN-treated *vs.* infected mice).

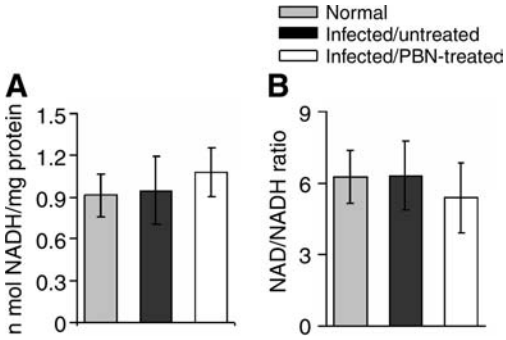

FIG. 3. Bar graphs showing the NADH level (A) and NAD^+/NADH ratio (B) in isolated cardiac mitochondria from normal, infected/untreated and infected/PBN-treated mice ($n = 9$ per group).

was not statistically different in isolated cardiac mitochondria of the three groups. These results indicate that mitochondrial oxygen uptake and substrate-dependent respiration were not compromised in infected myocardium. The RCR values of > 4.0 (Table 3) suggested that coupled mitochondria were isolated from infected myocardium. Yet, the ADP-stimulated state 3 respiration (indicates proton gradient for ATP synthesis) and ADP/O ratio (rate of ADP phosphorylation per O atom consumed) were substantially decreased in substrate-respiring cardiac mitochondria of infected mice (Fig. 4C and D). The deficiency of state 3 respiration and ADP phosphorylation was validated in heart tissue. Left ventricle (LV) sections from normal and infected mice were incubated with pyr/mal or succinate to energize mitochondria, and the rate of respiration was determined (Fig. 4E, data not shown). The substrate-dependent, endogenous ADP-stimulated, respiration in LV of infected mice was 38% lower than that of normal controls, and remained depressed with exogenous ADP addition. These data suggest that the electrochemical gradient required for ATP synthesis was compromised in infected myocardium. The observation that pyr/mal- and succinate-stimulated, but not ascorbate/TMPD-stimulated, state 3 respiration was decreased in infected cardiac mitochondria indicated that electron transport at complex IV and downstream (to complex V) was intact, and instead, the deficiencies of complex I or complex III or both contributed to decreased state 3 rate and ATP synthesis in infected myocardium.

TABLE 2. MITOCHONDRIAL ATP-PRODUCTION RATE IN THE MYOCARDIUM OF *T. CRUZI*-INFECTED MICE ± PBN

		Mitochondrial ATP synthesis rate (pmol/mg protein/min)							
Substrate	*Animals*	*None*	*6.5 μM Rot*	*2.5 mM Mal*	*10 μM Myx*	*10 μM Ant*	*1 mM KCN*	*12 μM Oligo*	*0.2 mM DNP*
Pyr/Mal	Normal	65.36 ± 3.65	6.17 ± 0.67	ND	6.50 ± 1.67	2.00 ± 0.33	0.72 ± 0.17	10.00 ± 1.67	2.00 ± 0.50
	IUT	32.83 ± 1.82[a]	3.83 ± 0.67	ND	4.33 ± 1.33	4.00 ± 0.83	0.67 ± 0.17	7.00 ± 0.67	1.00 ± 0.50
	IPBNT	56.19 ± 2.4[b]	3.67 ± 2.83	ND	4.50 ± 0.17	2.67 ± 0.17	1.00 ± 0.12	8.50 ± 3.67	1.83 ± 1.50
Succinate	Normal	34.98 ± 5.37	ND	2.50 ± 0.50	1.17 ± 0.50	5.00 ± 0.33	1.50 ± 0.67	10.33 ± 2.00	−0.17 ± 0.17
	IUT	19.74 ± 4.21[a]	ND	1.33 ± 0.50	0.50 ± 0.50	3.67 ± 0.50	0.50 ± 0.33	4.50 ± 0.33	−0.83 ± 0.67
	IPBNT	32.27 ± 6.79[b]	ND	1.50 ± 0.50	1.17 ± 0.50	8.50 ± 0.83	0.83 ± 0.33	8.00 ± 1.00	0.08 ± 0.33

Cardiac mitochondria from normal, infected/untreated (IUT) and infected/PBN-treated (IPBNT) mice were isolated as described in Materials and Methods. Mitochondria were incubated at room temperature with the indicated substrates (with or without inhibitors), and the ATP-production rate was determined by luciferin/luciferase-based luminescence assay. The data (mean ± SD) are representative of three independent experiments (n = 3 per experiment/group). Pyr/Mal, pyruvate/malate. Inhibitors: Rot, rotenone (CI); Mal, malonate (CII); Myx, myxothiazol (CIII); Ant, antimycin A (CIII); KCN, (CIV); Oligo, oligomycin (CV); DNP, dinitrophenol (uncoupler). The level of significance is shown by $^{a}p < 0.001$ (normal *vs.* infected/untreated (IUT) mice) and $^{b}p < 0.001$ (infected/untreated *vs.* infected/PBN-treated (IPBNT) mice). ND, not determined.

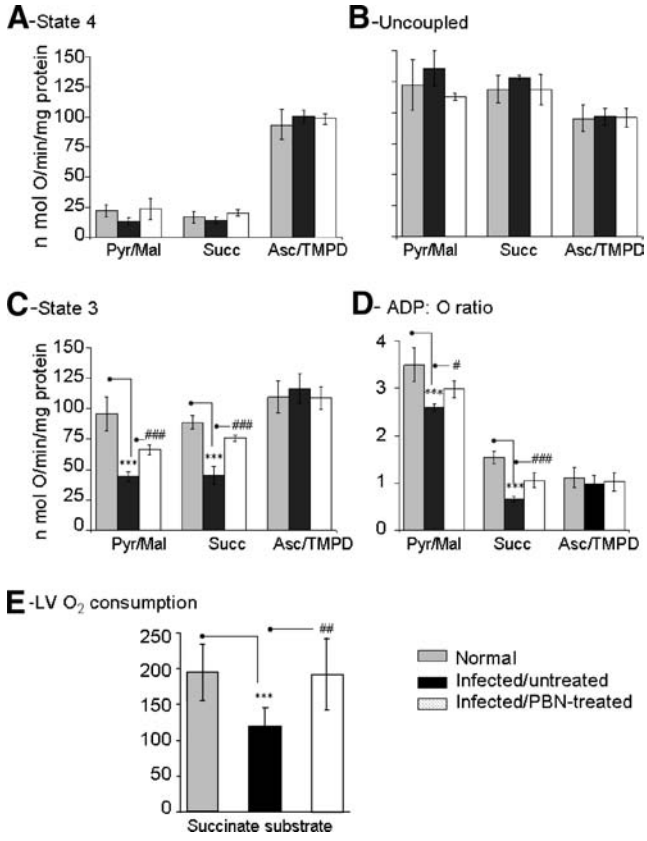

FIG. 4. Respiratory properties of cardiac mitochondria from *T. cruzi*–infected mice (±PBN). (**A**) State 4 respiration in isolated cardiac mitochondria of normal, infected, and infected/PBN-treated mice when pyruvate/malate (pyr/mal), succinate (succ), or ascorbate/TMPD (asc/TMPD) were used as substrates. (**B**) DNP-induced uncoupled (Unc) respiration rate. (**C**) The rate of state 3 respiration was determined after addition of ADP. (**D**) The ADP/O ratio (amount of ADP phosphorylated to O atom consumed) was calculated by measuring the decrease in O_2 concentration during state 3 respiration when 230 μM ADP was added. (**E**) The hearts were harvested, perfused, and LV sections used for *ex vivo* determination of substrate-dependent, state 3 respiration stimulated by endogenous ADP ($^{*,\#}p < 0.05$; $^{**,\#\#}p < 0.01$; $^{***}p < 0.001$; $n = 9$ mice/group).

In PBN-treated/infected mice, the substrate stimulated state 3 respiration and the ADP/O ratio of isolated cardiac mitochondria were significantly improved (Fig. 4C and D). Likewise, the substrate-dependent respiration was normalized in the LV of PBN-treated/infected mice as compared with infected/untreated mice, both when endogenous ADP was used (Fig. 4E) and with exogenous ADP addition (data not shown). These results imply the role of ROS in respiratory inefficiency and compromised ATP production in infected myocardium.

To delineate whether complex I or III or both are the site of electron-transport chain inefficiency, we carried out titration studies in presence of specific inhibitors. The titration of complex I inhibition with rotenone (0–100 n*M*) and its effect on ATP synthesis are shown in Fig. 5. In normal heart mitochondria, we observed rotenone concentration–dependent proportional decline in complex I activity and state 3 and ATP synthesis rates (Fig. 5A). The state 3 and ATP synthesis rates dropped by 58% and 22%, respectively, when complex I inhibition of 43% (from 198.4 to 113.1 nmol NADH oxidized/min/mg protein) was achieved with 30 n*M* rotenone (Fig. 5A). In infected myocardium, we found a 39%, 54% and 50% decline in mitochondrial complex I activity, state 3 respiration (44.4 ± 3.9 *vs.* 95.9 ± 14.0 nmol O/min/mg protein; $p < 0.001$) and ATP synthesis (32.8 ± 1.8 *vs.* 65.4 ± 3.6 pmol ATP/min/mg protein; $p < 0.001$), respectively, when compared with normal controls (Fig. 5B and C). Rotenone-induced further inhibition of complex I in cardiac mitochondria of infected mice corresponded to a similar pattern of respiration change, as was noted in normal controls (Fig. 5B). ATP synthesis in infected myocardial mitochondria was less sensitive to further inhibition of complex I activity (Fig. 5C). PBN treatment normalized the complex I activity in infected mice (Fig. 5B and C). However, the state 3 respiration (Fig. 5B), ATP production (Fig. 5C), and ADP/O ratio (Table 3) were only partially improved. The diminished state 3 and ATP synthesis rates and ADP/O ratio despite normalization of complex I activity by PBN treatment suggests that factors additional to complex I inhibition contributed to compromised respiration and ATP synthesis in infected mice.

Next, we titrated the complex III inhibition and its effect on respiration and ATP synthesis. Treatment with antimycin (0–100 n*M*) resulted in a proportional decline in complex III activity, state 3 rate, and ATP production in succinate-respiring normal cardiac mitochondria (Fig. 6A). Threshold curves showed that complex III inhibition of 67% (from 424.1 ± 47.1 to 140.9 ± 12.6 nmol cyt c oxidized/min/mg protein) was required before a 49% decline in state 3 rate (from 88.9 ± 5.1 to 45.7 ± 12.4 nmol O/min/mg protein) occurred (Fig. 6B). The ATP production rate was more sensitive to complex III inhibition. A 16% loss in complex III activity (from 424.1 ± 47.2 to 357.9 ± 45.0 nmol cyt c oxidized/min/mg protein) resulted in a 67% decline in ATP synthesis rate (from 35.0 ± 5.4 to 11.4 ± 2.0 pmol ATP/min/mg protein) in normal cardiac mitochondria (Fig. 6C). In infected myocardium, complex III activity was decreased by 59%. This loss in complex III activity in infected myocardial mitochondria corresponded to a 49% decline in respiration (45.3 ± 7.3 *vs.* 88.8 ± 5.1 nmol O/min/mg protein) and 44% decline in ATP production (19.7 ± 4.2 *vs.* 35.0 ± 5.4 pmol ATP/min/mg protein; $p < 0.001$) than normal controls (Fig. 6B and C; Tables 2 and 3). Antimycin-induced further inhibition of complex III resulted in a sharp decline in the state 3 and ATP production rates in infected myocardium (Fig. 6B and C). PBN treatment of infected mice recovered 58% loss of complex III activity (Fig. 6B and C) (42) that was associated with normalized state 3 respiration (Fig. 6B) and a substantial increase in ATP synthesis (Fig. 6C) and ADP/O ratio (Table 3). The sensitivity of the ATP synthesis rate to complex III inhibition in infected mice and the improvement in respiration and ATP production with preservation of complex III activity in PBN-treated/infected mice suggest that compromised respiratory efficiency and ATP synthesis are an outcome of complex III inhibition in chagasic myocardium.

Considering the beneficial effects of PBN (Fig. 6) and our recent observations documenting that complex III is the site for increased electron leakage to molecular oxygen (46), we considered that ROS contributed to mitochondrial loss of complex III activity in infected myocardium. The mtDNA,

Table 3. Respiratory Parameters of Heart Mitochondria from Mice Infected with *T. cruzi* ± PBN

Substrate	Animals	Rate of respiration (nmol atom O/min/mg protein)			RCR value (state 3/state 4)	ADP/O
		State 4 (−ADP)	State 3 (+ADP)	DNP-stimulated		
Pyruvate$^+$ malate	Normal	21.89 ± 5.11	95.95 ± 14.01	121.92 ± 20.3	4.54 ± 1.32	3.36 ± 0.40
	T. cruzi infected	13.30 ± 2.83	44.42 ± 3.94[a]	135.33 ± 14.31	4.11 ± 0.4	2.69 ± 0.17[b]
	Infected/PBN-treated	23.58 ± 8.98	66.32 ± 4.15[c]	112.57 ± 2.56	3.62 ± 0.53	2.92 ± 0.37
Succinate$^+$ rotenone	Normal	16.43 ± 4.96	88.85 ± 5.14	118.63 ± 10.96	5.55 ± 1.49	1.54 ± 0.125
	T. cruzi-infected	14.13 ± 2.26	45.34 ± 7.3[a]	127.81 ± 1.66	4.44 ± 1.51	0.66 ± 0.05[a]
	Infected/PBN-treated	19.95 ± 3.99	76.04 ± 2.66[c]	118.05 ± 12.3	5.53 ± 0.87	1.05 ± 0.20c
Ascorbate$^+$ TMPD	Normal	93.36 ± 12.64	109.53 ± 13.15	94.98 ± 10.59	1.19 ± 0.05	1.12 ± 0.21
	T. cruzi-infected	100.58 ± 5.1	116.55 ± 12.08	96.74 ± 6.88	1.16 ± 0.15	0.98 ± 0.18
	Infected/PBN-treated	98.24 ± 4.15	105.92 ± 9.42	95.64 ± 7.58	1.12 ± 0.09	1.03 ± 0.2

Cardiac mitochondria were isolated as described in Material and Methods. Mitochondria were incubated with the indicated substrates, and the respiration rate was determined by oxygraphy. ADP/O ratio represents the nmol ADP phosphorylated per ng atom of oxygen consumed. DNP, dinitrophenol; NA, not applicable; RCR, respiratory control ration. The data (mean ± SD) are representative of three independent experiments (*n* three mice per experiment/group). [b]$p < 0.05$; [a]$p < 0.001$ (normal *vs.* infected mice), [c]$p < 0.001$ (infected/PBN treated mice *vs.* infected mice).

highly susceptible to oxidative damage encodes the cyt b subunit of the complex III. Southern blotting (Fig. 7A and B) and real-time PCR (Fig. 7C) showed that *cyt b* DNA was significantly decreased in infected murine hearts as compared with normal controls. The cyt b mRNA level was determined with Northern blotting (Fig. 7D and E) and traditional (not shown) and real-time (Fig. 7F) RT-PCR. All three techniques showed about an 80% decline in cyt b mRNA levels in infected murine hearts. Subsequently, Western blot analysis showed the cyt b protein level decreased by 74% in cardiac mitochondria of infected mice as compared with normal controls (Fig. 7G and H).

To investigate whether decreased the cyt b level affected complex III in infected heart, we resolved the respiratory complexes on blue native gel, and performed catalytic staining and Western blot analysis to evaluate complex III assembly, activity, and cyt b incorporation. Our data showed that the assembly of complex III and other respiratory complexes occurred at a similar level in cardiac mitochondria of infected and normal mice (Fig. 8A). However, catalytic activity (40% decline, also validated by spectrophotometric observations) and cyt b level (61% decline; Fig. 8B and C) were decreased in the CIII complex of infected myocardium. PBN treatment of infected mice improved the cyt b DNA, mRNA, and protein levels (Fig. 7). Subsequently, the complex III cyt b level (Fig. 8) and catalytic activity were restored in PBN-treated/infected mice. Together, these results suggest that decreased expression of mtDNA-encoded cyt b contributed to complex III inhibition in cardiac mitochondria of *T. cruzi*–infected mice, and this defect was alleviated by PBN treatment.

Discussion

We used a murine model of *T. cruzi* infection in this study that exhibits characteristics of human chagasic disease. Experimentally infected mice elicit reproducible and

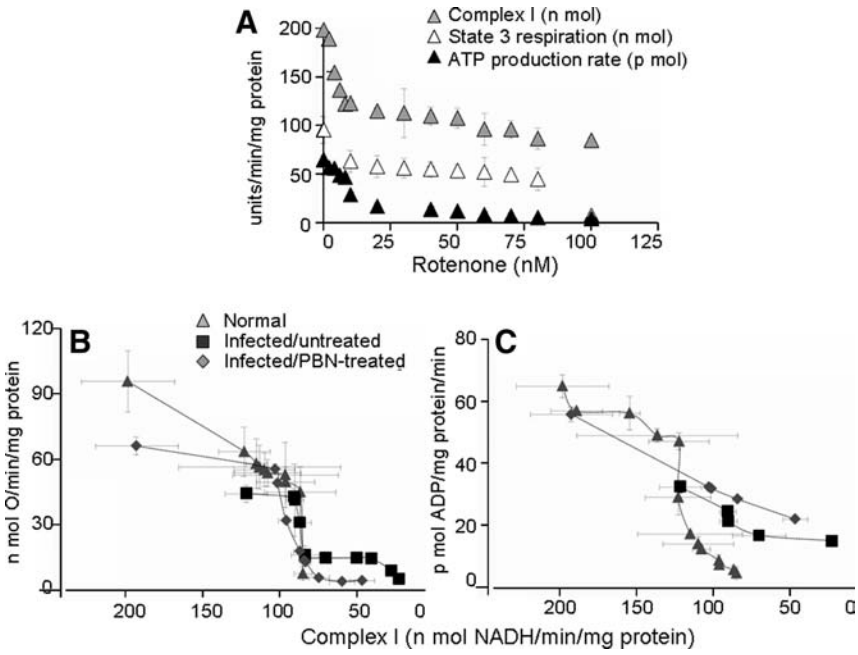

FIG. 5. Titration of complex I inhibition and its effect on respiration and ATP-production rate in cardiac mitochondria of *T. cruzi*–infected mice. Freshly isolated cardiac mitochondria were incubated with rotenone (0–100 n*M*) and energized with pyr/mal substrates. (**A**) Effects of rotenone on complex I activity, state 3 respiration, and ATP-production rate in normal heart mitochondria. Threshold curves show the effect of rotenone-induced changes in complex I–specific activity on the state 3 (**B**) and ATP-production (**C**) rates in isolated cardiac mitochondria from normal, infected/untreated, and infected/PBN-treated mice. Data (mean ± SD) are representative of three independent experiments ($n = 9$ mice per group).

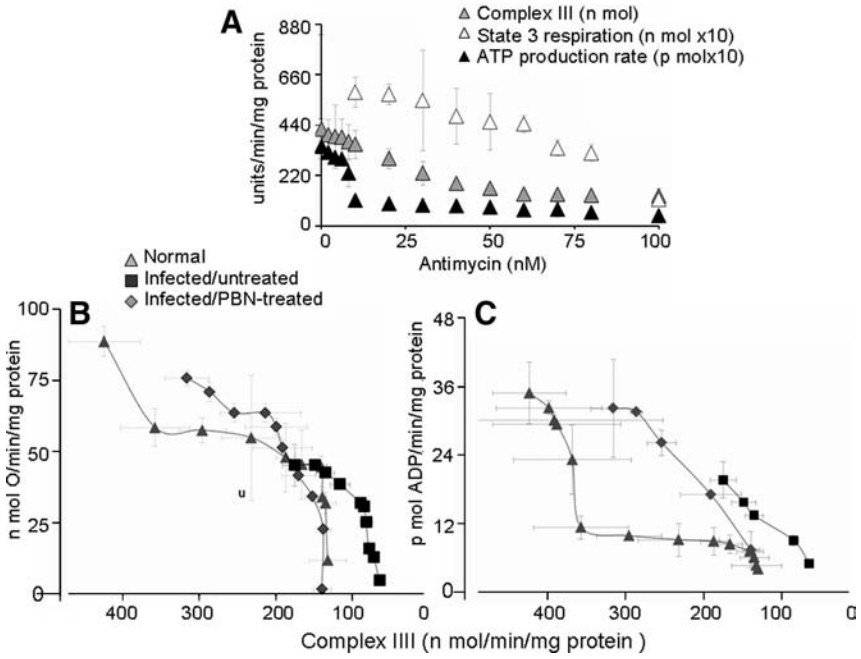

FIG. 6. Titration of complex III inhibition and its effect on respiration and ATP-production rate in cardiac mitochondria of *T. cruzi*–infected mice. Freshly isolated cardiac mitochondria were incubated with antimycin (0–100 n*M*) and energized with succinate. (**A**) Effects of antimycin on CIII activity, state 3, and ATP-production rate in normal heart mitochondria. Threshold curves show the effect of antimycin-induced changes in complex III activity on the state 3 (**B**) and ATP-production (**C**) rates in cardiac mitochondria from normal, infected/untreated, and infected/PBN-treated mice. Data (mean ± SD) are representative of three independent experiments ($n = 9$ mice per group).

comparable acute disease associated with parasitemia (tissues parasites). The presence of myocarditis and focal necrosis elicits the acute disease in mice (13, 45) similar to acute infection in humans (2). Tissue damage and fibrosis associated with diffused inflammation become prominent during the chronic phase (13). Symptomatic defects include cardiomegaly, diffused myocarditis, self-perpetuating myofibril destruction, and a decline in LV ejection fraction (9, 26, 36), a picture reminiscent of the chronic form of Chagas disease observed in humans (24, 25).

Moderate-to-severe electrocardiographic and echocardiographic alterations evident in rodent hearts (3, 7) are

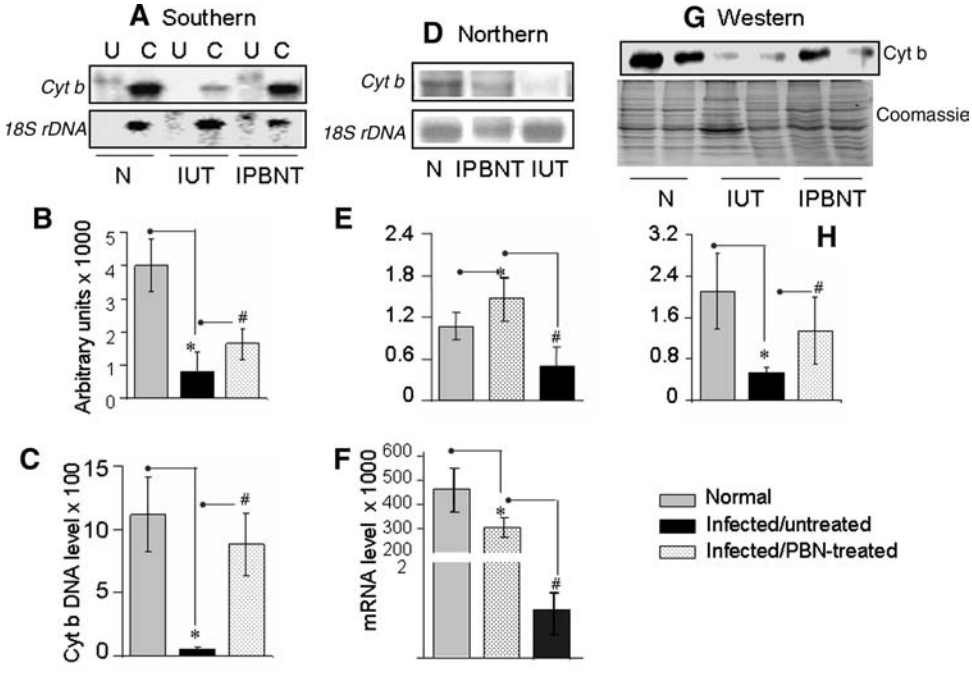

FIG. 7. Expression of cytochrome b is altered in the myocardium of *T. cruzi*–infected mice. Total DNA and total RNA were isolated from myocardial tissue of normal (N), infected/untreated (IUT), and infected/PBN-treated (IPBNT) mice. (**A**, **B**) Southern blotting. Total genomic DNA (3 μg; U, uncut; **C**, *Eco*RI digested) was resolved on agarose gel and hybridized with a [^{32}P]-labeled sequence for cyt b or 18S rRNA (**A**). Densitometric analysis of cyt b DNA signal, normalized with 18S rDNA signal (**B**). (**C**) A real-time PCR was performed to measure the *cyt b* DNA level, normalized to *GAPDH*. (**D, E**) Northern blot analysis. Total RNA (2.5 μg) was resolved on gel and hybridized with [^{32}P]-labeled cDNA probes for *cyt b* or 18S rRNA (**D**). Densitometric analysis of *cyt b* mRNA signal, normalized with 18S rRNA signal (**E**). (**F**) A real-time RT-PCR was performed to measure the *cyt b* mRNA level, normalized to *GAPDH* cDNA. Data in **C** and **F** represent mean $2^{-\Delta Ct}$ values obtained from two independent experiments ($n = 6$). The standard deviation for all the data points was <10% ($p < 0.05$). (**G**, **H**) Mitochondrial lysates (15 μg protein) were resolved by SDS-PAGE, and Western blot analysis was performed by using an anti-cyt b antibody (**G**). Membranes were stained with Coomassie R250 to confirm equal loading of the samples. Densitometric analysis of cyt b protein is shown in (**H**). Data in **B**, **E**, and **H** represent mean ± SD ($n = 9$ mice per group; $^{*,\#}p < 0.001$).

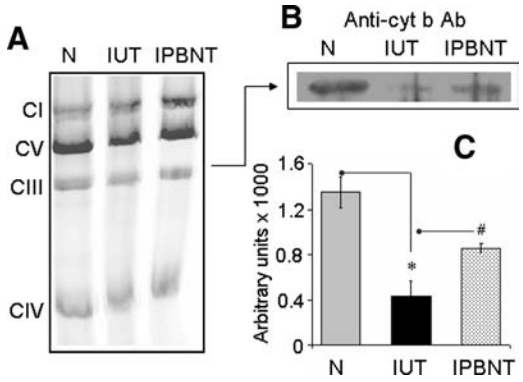

FIG. 8. Assembly of cytochrome *b*–depleted complex III in infected myocardium. (**A**) Isolated mitochondria (50 μg protein) from normal (N), infected/untreated (IUT), and infected/PBN-treated (IPBNT) mice were subjected to blue-native gel electrophoresis, and respiratory complexes were resolved. (**B**) Complex III from the blue native gel was subjected to second-dimension SDS-PAGE to resolve the subunit components, and Western blotting was performed by using an anti-cyt b antibody. (**C**) Densitometric analysis of cyt b protein, normalized to complex III level ($^{*,\#}p < 0.001$).

associated with electrical conduction disturbances, diastolic dysfunction, lower O_2 consumption, and anaerobic threshold (26). We and others have shown that myocardial energetics and ATP content were compromised in infected rodents (38, 42). Our observations in this study demonstrating that the oxygen consumption, state 3 rate, ATP production, and ADP-to-O ratio were decreased in LV and isolated cardiac mitochondria of infected mice provide the first molecular evidence for mitochondrial decline in oxidative phosphorylation in chagasic hearts.

What might contribute to the observed decline in mitochondrial ATP production in infected mice? Parasite-induced cellular injuries can result in isolation of damaged uncoupled mitochondria. In coupled mitochondria, complexes of the electron transport chain (ETC) create a transmembrane electrochemical gradient ($\Delta\psi$). Complex V (ATP synthase) uses the potential energy stored in $\Delta\psi$ to phosphorylate ADP. The $\Delta\psi$ can collapse to result in the free diffusion of molecules between the matrix and the cytosol (17). Reports of electron microscopic analysis of biopsies from experimental animals have indicated that a degree of mitochondrial structural damage occurs in infected myocardium (13), thus suggesting that mitochondria in infected heart may just be uncoupled. However, a high RCR value (>4.0; Table 3) indicated that the electron-transport chain and oxidative phosphorylation were coupled in mitochondria of infected mice. Another plausible mechanism of decreased ATP production and ATP content is the unavailability of intermediary metabolites (*e.g.*, NADH for complex I or $FADH_2$ for complex II) for maintaining the electrochemical gradient across the respiratory chain. Pyruvate/malate substrates provide NADH to the complex I that pumps electrons to CoQ. From CoQ, electrons are transferred to O_2 at the complex IV with coupled ATP synthesis in the presence of ADP (15). Succinate dehydrogenase (SDH) provides $FADH_2$ to complex II, from which electrons flow through complex III and complex IV. The mitochondrial NADH level and NAD^+/NADH ratio were not decreased in infected myocardium (Fig. 3), and the impaired state 3 respiration of infected cardiac mitochondria was not relieved when exogenous NADH was added. Likewise, we observed no change in SDH activity in infected myocardium (41). These observations suggest that an impaired ATP production in infected myocardium was not due to a reduced availability of intermediary metabolites (NADH, $FADH_2$) that provide electron energy for mitochondrial ATP synthesis.

The perturbations in electron-transport chain efficiency and complex V activity can also result in decreased bioenergetics in the heart. Reduced ATP synthesis, as measured by a declining state 3 rate, has been demonstrated in isolated cardiac mitochondria from failing animal (31) and human hearts (32). Others have attributed the disease pathology in cardiac failure during ischemia/reperfusion (37) and in neurologic and age-related diseases [*e.g.*, Alzheimer's (1), Parkinson's, and Huntington's (30)] to a loss in respiratory-complex activities and postulated that a lack of ATP production ensues. However, skepticism exists concerning a direct correlation between decline in complex activities and ATP synthesis in a disease condition. This is because mitochondrial respiratory complexes harbor more capacity than is required to maintain electron transport and ATP synthesis for normal cardiac function (27, 28). Thus, a decline in a complex activity, if not sufficient to exhaust the reserve capacity, would not be physiologically relevant and would have no adverse effects on electron transport and ATP-production capacity. Our finding that rotenone inhibition of complex I by 39% had no effect on ATP production in normal cardiac mitochondria (Fig. 5), suggests that a similar percentage loss of complex I activity in infected myocardium (41, 42) was physiologically irrelevant and did not contribute to decreased ATP synthesis in infected myocardium. Likewise, a small, but statistically significant decline in complex IV and complex V activities in chagasic heart (41, 42) was not physiologically relevant. This was evident by the observation that infected myocardial mitochondria respiring TMPD/ascorbate substrates (donate electrons to complex IV) exhibited no decline in state 3 respiration and ADP-to-O ratio (Fig. 4D; Table 3). Others have reported that the kinetics of ATP synthesis/ATP hydrolysis by complex V was not altered in rats acutely infected by *T. cruzi* (39). Thus, the capacity of complex IV to transfer electrons and the ability of complex V to receive electrochemical gradient energy and synthesize ATP were not affected in cardiac mitochondria of infected mice.

Instead, the ATP production rate was highly sensitive to the complex III inhibition (Fig. 6). The titration assay showed that antimycin-induced inhibition of complex III by 16% resulted in 67% loss in ATP production in normal cardiac mitochondria. In infected mice, a 59% inhibition of complex III activity was observed, and it corresponded to a 44% loss in mitochondrial ATP production (Fig. 6; Table 2). PBN treatment resulted in a substantial improvement in the mitochondrial activity of complex III, state 3 respiration, ATP production, and ADP/O ratios in infected myocardium. Others noted the biochemical threshold value of respiratory complexes decreases with aging (40). We surmise that mitochondrial perturbations of complex III affected ATP production in infected myocardium, and these disturbances will likely be exacerbated during the chronic-disease phase when patients are older and may develop age-related respiratory inefficiency.

Cytochrome *b*, together with cyt c_1 and the iron-sulfur protein (ISP), forms the catalytic core of the CIII complex (5). The Q cycle receives electrons from complex I and complex II,

and cytochrome *b* acts as a bridge for electron transfer from Q cycle to complex IV (10). The mtDNA encoded cyt b was decreased in infected myocardium (Figs. 7 and 8), whereas expression levels for other components of the complex III were not altered in infected heart (43). These observations allow us to propose that in the absence of cytochrome *b*, complex III would not efficiently receive the electrons coming from complex I (when mitochondria are respiring pyr/mal) and complex II (when mitochondria are respiring succinate) and pump them to the complex IV. The inefficient transfer of electrons from complex III to complex IV would affect the coupled ATP synthesis.

In summary, we demonstrated that the myocardial bioenergetics decline during *T. cruzi* infection occurs because of inefficient electron transport for ATP synthesis in mitochondria. A decline in cyt b expression caused a loss in complex III activity and constituted a mechanism for decreased mitochondrial state 3 respiration and ATP production in the myocardium of infected mice. Treatment with PBN improved the cyt b expression, complex III activity, mitochondrial respiration, and ATP production in the myocardium of *T. cruzi*–infected mice.

Acknowledgments

This work was supported by a grant (AI054578) from the National Institute of Allergy and Infectious Diseases/ National Institutes of Health to N.J.G.

Author Disclosure Statement

No competing financial interests exist.

References

1. Aleardi AM, Benard G, Augereau O, Malgat M, Talbot JC, Mazat JP, Letellier T, Dachary–Prigent J, Solaini GC, and Rossignol R. Gradual alteration of mitochondrial structure and function by beta-amyloids: importance of membrane viscosity changes, energy deprivation, reactive oxygen species production, and cytochrome c release. *J Bioenerg Biomembr* 37: 207–225, 2005.
2. Andrade ZA. Pathogenesis of Chagas disease. *Res Immunol* 142: 126–129, 1991.
3. Bilate AM, Salemi VM, Ramires FJ, de Brito T, Russo M, Fonseca SG, Fae KC, Martins, DG, Silva AM, Mady C, Kalil J, and Cunha-Neto. TNF blockade aggravates experimental chronic Chagas disease cardiomyopathy. *Microb Infect* 9: 1104–1113, 2007.
4. Báez AL, Lo Presti, MS, Rivarola HW, Pons P, Fretes R, and Paglini-Oliva P. *Trypanosoma cruzi*: cardiac mitochondrial alterations produced by different strains in the acute phase of the infection. *Exp Parasitol* 120: 397–402, 2008.
5. Brasseur G, Saribas AS, and Daldal F. A compilation of mutations located in the cytochrome b subunit of the bacterial and mitochondrial bc1 complex. *Biochim Biophys Acta* 1275: 61–69, 1996.
6. Brener Z and Gazzinelli RT. Immunological control of *Trypanosoma cruzi* infection and pathogenesis of Chagas' disease. *Int Arch Allergy Immunol* 114: 103–110, 1997.
7. Bustamante JM, Rivarola HW, Fretes R, and Paglini-Oliva PA. Weekly electrocardiographic pattern in mice infected with two different *Trypanosoma cruzi* strains. *Int J Cardiol* 102: 211–217, 2005.
8. Chomczynski P and Sacchi N. Single-step method of RNA isolation by acid guanidinium thiocyanate-phenol-chloroform extraction. *Anal Biochem* 162: 156–159, 1987.
9. de Souza AP, Tang B, Tanowitz HB, Araujo-Jorge TC, and Jelicks EL. Magnetic resonance imaging in experimental Chagas disease: a brief review of the utility of the method for monitoring right ventricular chamber dilatation. *Parasitol Res* 97: 87–90, 2005.
10. di Rago JP, Netter P, and Slonimski PP. Intragenic suppressors reveal long distance interactions between inactivating and reactivating amino acid replacements generating three-dimensional constraints in the structure of mitochondrial cytochrome b. *J Biol Chem* 265: 15750–15757, 1990.
11. Floyd RA, Hensley K, Forster MJ, Kelleher-Anderson JA, and Wood PL. Nitrones as neuroprotectants and antiaging drugs. *Ann N Y Acad Sci* 959: 321–329, 2002.
12. Garg N, Bhatia V, Gerstner A, deFord J, and Papaconstantinou J. Gene expression analysis in mitochondria from chagasic mice: alterations in specific metabolic pathways. *Biochemical J* 381:743–752, 2004.
13. Garg N, Popov VL, and Papaconstantinou J. Profiling gene transcription reveals a deficiency of mitochondrial oxidative phosphorylation in *Trypanosoma cruzi*-infected murine hearts: implications in chagasic myocarditis development. *Biochim Biophys Acta* 1638: 106–120, 2003.
14. Harper AE. Glucose-6-phosphatase. In: *Methods of Enzymatic Analysis*, edited by Bergmeyer HU. New York: Academic Press Inc., 1965, pp. 788–792.
15. Jafri MS, Dudycha SJ, and O'Rourke B. Cardiac energy metabolism: models of cellular respiration. *Annu Rev Biomed Eng* 3: 57–81, 1963.
16. Kawaguchi AT, Sugimachi M, Sunagawa K, Bergsland J, Koide S, and Batista RJ. Improved left ventricular contraction and energetics in a patient with Chagas' disease undergoing partial left ventriculectomy. *J Card Surg* 16: 30–33, 2001.
17. Kokoszka JE, Coskun P, Esposito LA, and Wallace DC. Increased mitochondrial oxidative stress in the Sod2 (+/−) mouse results in the age-related decline of mitochondrial function culminating in increased apoptosis. *Proc Natl Acad Sci U S A* 98: 2278–2283, 2001.
18. Lemasters JJ. The ATP-to-oxygen stoichiometries of oxidative phosphorylation by rat liver mitochondria: an analysis of ADP-induced oxygen jumps by linear nonequilibrium thermodynamics. *J Biol Chem* 259: 13123–13130, 1984.
19. Leonardo MR, Dailly Y, and Clark DP. Role of NAD in regulating the adhE gene of *Escherichia coli*. *J Bacteriol* 178: 6013–6018, 1996.
20. Loke KE, Laycock SK, Mital S, Wolin MS, Bernstein R, Oz M, Addonizio L, Kaley G, and Hintze TL. Nitric oxide modulates mitochondrial respiration in failing human heart. *Circulation* 100: 1291–1297, 1991.
21. Lui NS, Roels OA, Trout ME, and Anderson OR. Subcellular distribution of enzymes in *Ochromonas malhamensis*. *J Protozool* 15: 536–542, 1968.
22. Palacios-Pru E, Carrasco H, Scorza C, and Espinoza R. Ultrastructural characteristics of different stages of human chagasic myocarditis. *Am J Trop Med Hyg* 41: 29–40, 1989.
23. Parada H, Carrasco HA, Anez N, Fuenmayor C, and Inglessis I. Cardiac involvement is a constant finding in acute Chagas' disease: a clinical, parasitological and histopathological study. *Int J Cardiol* 60: 49–54, 1997.
24. Rassi A Jr, Rassi A, and Little WC. Chagas' heart disease. *Clin Cardiol* 23: 883–889, 2000.

25. Rassi A Jr, Rassi A, Little WC, Xavier SS, Rassi SG, Rassi GG, Hasslocher-Moreno A, Sousa AS, and Scanavacca MI. Development and validation of a risk score for predicting death in Chagas' heart disease. *N Engl J Med* 355: 799–808, 2006.
26. Rocha NN, Garcia S, Gimenez LE, Hernandez CC, Senra JF, Lima RS, Cyrino F, Bouskela E, Soares MB, Ribeiro dos Santos R, and Campos de Carvalho AC. Characterization of cardiopulmonary function and cardiac muscarinic and adrenergic receptor density adaptation in C57BL/6 mice with chronic *Trypanosoma cruzi* infection. *Parasitology* 133: 729–737, 2006.
27. Rossignol R, Faustin B, Rocher C, Malgat M, Mazat JP, and Letellier T. Mitochondrial threshold effects. *Biochem J* 370: 751–762, 2003.
28. Rossignol R, Malgat M, Mazat JP, and Letellier T. Threshold effect and tissue specificity: implication for mitochondrial cytopathies. *J Biol Chem* 274: 33426–33432, 1999.
29. Schagger H. Native electrophoresis for isolation of mitochondrial oxidative phosphorylation protein complexes. *Methods Enzymol* 260: 190–202, 1995.
30. Schapira AH. Mitochondrial involvement in Parkinson's disease, Huntington's disease, hereditary spastic paraplegia and Friedreich's ataxia. *Biochim Biophys Acta* 1410: 159–170, 1999.
31. Sharov VG, Goussev A, Lesch M, Goldstein S, and Sabbah HN. Abnormal mitochondrial function in myocardium of dogs with chronic heart failure. *J Mol Cell Cardiol* 30: 1757–1762, 1998.
32. Sharov VG, Todor AV, Silverman N, Goldstein S, and Sabbah HN. Abnormal mitochondrial respiration in failed human myocardium. *J Mol Cell Cardiol* 32: 361–367, 2000.
33. Sheeran FL and Pepe S. Energy deficiency in the failing heart: linking increased reactive oxygen species and disruption of oxidative phosphorylation rate. *Biochim Biophys Acta* 1757: 543–552, 2006.
34. Sims NR and Anderson MF. Isolation of mitochondria from rat brain using Percoll density gradient centrifugation. *Nat Protoc* 3: 1228–1239, 2008.
35. Slater EC. Mechanism of oxidative phosphorylation. *Annu Rev Biochem* 46: 1015–1026, 1977.
36. Teixeira ARL, Nascimento RJ, and Sturm N. Evolution and pathology in Chagas disease: a review. *Mem Inst Oswaldo Cruz* 101: 463–449, 2006.
37. Towbin JA, Bowles KR, and Bowles NE. Etiologies of cardiomyopathy and heart failure. *Nat Med* 5: 266–267, 1999.
38. Uyemura SA, Albuquerque A, and Curti C. Energetics of heart mitochondria during acute phase of *Trypanosoma cruzi* infection in rats. *Int J Biochem Cell Biol* 27: 1183–1189, 1995.
39. Uyemura SA, Jordani MC, Polizello AC, and Curti C. Heart FoF1-ATPase changes during the acute phase of *Trypanosoma cruzi* infection in rats. *Mol Cell Biochem* 165: 127–133, 1996.
40. Ventura B, Genova ML, Bovina C, Formiggini G, and Lenaz G. Control of oxidative phosphorylation by Complex I in rat liver mitochondria: implications for aging. *Biochim Biophys Acta* 1553: 249–260, 2002.
41. Vyatkina G, Bhatia V, Gerstner A, Papaconstantinou J, and Garg N. Impaired mitochondrial respiratory chain and bioenergetics during chagasic cardiomyopathy development. *Biochim Biophys Acta* 1689: 162–173, 2004.
42. Wen J-J, Bhatia V, Popov VL, and Garg NJ. Phenyl-alpha-tert-butyl nitrone reverses mitochondrial decay in acute Chagas disease. *Am J Pathol* 169: 1953–1964, 2006.
43. Wen J-J and Garg N. Oxidative modifications of mitochondrial respiratory complexes in response to the stress of *Trypanosoma cruzi* infection. *Free Radic Biol Med* 37: 2072–2081, 2004.
44. Wen J-J, Vyatkina G, and Garg N. Oxidative damage during chagasic cardiomyopathy development: role of mitochondrial oxidant release and inefficient antioxidant defense. *Free Radic Biol Med* 37: 1821–1833, 2004.
45. Wen J-J, Dhiman M, Whorton EB, Garg NJ. Tissue-specific oxidative imbalance and mitochondrial dysfunction during *Trypanosoma cruzi* infection in mice. *Microbes Infect* 10: 1201–1209, 2008.
46. Wen J-J and Garg NJ. Mitochondrial generation of reactive oxygen species is enhanced at the Q(o) site of the complex III in the myocardium of *Trypanosoma cruzi*-infected mice: beneficial effects of an antioxidant. *J Bioenerg Biomembr* 40: 587–598, 2008.
47. World Health Organization. Control of Chagas disease: second report of the WHO expert committee. Geneva, Switzerland, UNDP/World Bank/WHO, 2002.
48. Wibom R, Lundin A, and Hultman E. A sensitive method for measuring ATP-formation in rat muscle mitochondria. *Scand J Clin Lab Invest* 50: 143–152, 1990.

Address correspondence to:
Dr. Nisha Jain Garg
3.142C Medical Research Building
University of Texas Medical Branch
301 University Boulevard
Galveston TX 77555-1070

E-mail: nigarg@utmb.edu

Date of first submission to ARS Central, December 19, 2008; date of final revised submission, July 21, 2009; date of acceptance, July 22, 2009.

Abbreviations Used

APase = acid phosphatase
Asc/TMPD = ascorbate/*N,N,N,N*-tetramethyl-*p*-phenylenediamine
complex I = NADH ubiquinone oxidoreductase
complex II = succinate decylubiquinone 2,6-dichlorophenolindophenol reductase
complex III = ubiquinol cytochrome *c* oxidoreductase
complex IV = cytochrome *c* oxidase
CS = citrate synthase
cyt b = cytochrome *b*
cyt c = cytochrome *c*
DB = 2,3- dimethoxy-5-methyl-6-decyl-1, 4-benzoquinone
GAPDH = glyceraldehyde-3-phosphate dehydrogenase
G-6-Pase = glucose-6-phosphatase
PBN = phenyl-*α*-*tert*-butyl nitrone
pyr/mal = pyruvate/malate
RCR = respiratory control ratio
ROS = reactive oxygen species
suc/rot = succinate/rotenone
T. cruzi = *Trypanosoma cruzi*